JACS
JOURNAL OF THE AMERICAN CHEMICAL SOCIETY
Article
pubs.acs.org/JACS

Synthesis, Crystal Structure and Magnetic Properties of the New One-Dimensional Manganate $Cs_3Mn_2O_4$

Jürgen Nuss,[†] Maria A. Señaris-Rodriguez,[†,‡] Prasad L. V. K. Dasari,[†,§] Moritz Stahl,[†] and Martin Jansen*[,†]

[†]Max Planck Institute for Solid State Research, Heisenbergstrasse 1, 70569 Stuttgart, Germany
[‡]Dpto Química Fundamental, Facultad de Ciencias, Universidad de A Coruña, 15071 A Coruña, Spain
[§]Department of Chemistry and Chemical Biology, Cornell University, Ithaca, New York 14853, United States

Supporting Information

ABSTRACT: $Cs_3Mn_2O_4$, a new member of the small family of ternary manganese (II/III) mixed-valent compounds, has been synthesized via the azide/nitrate route and studied using powder and single crystal X-ray diffraction, magnetic susceptibility measurements and density functional theory (DFT). Its crystal structure ($P2_1/c$, Z = 8, a = 1276.33(1) pm, b = 1082.31(2) pm, c = 1280.29(2) pm, β = 118.390(2)°) is based on one-dimensional $MnO_2^{1.5-}$ chains built up from edge-sharing MnO_4 tetrahedra. The title compound is the first example of an intrinsically doped transition metalate of the series A_xMnO_2, (A = alkali metal) where a complete 1:1 charge ordering of Mn^{2+} and Mn^{3+} is observed along the chains ($-Mn^{2+}-Mn^{3+}-Mn^{2+}-Mn^{3+}-$). From the magnetic point of view it basically consists of ferrimagnetic MnO_2 chains, where the Mn^{2+} and Mn^{3+} ions are strongly antiferromagnetically coupled up to high temperatures. Very interestingly, their long-range three-dimensional ordering below the Néel temperature (T_N) ~12 K give rise to conspicuous field dependent magnetic ordering phenomena, for which we propose a consistent picture based on the change from antiferromagnetic to ferromagnetic coupling between the chains. Electronic structure calculations confirm the antiferromagnetic ordering as the ground state for $Cs_3Mn_2O_4$ and ferrimagnetic ordering as its nearly degenerate state.

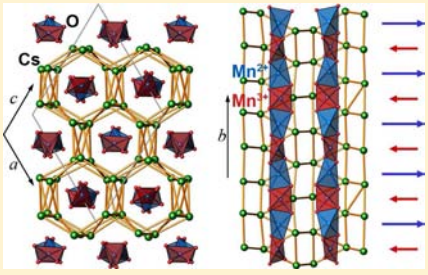

INTRODUCTION

Particular electronic and magnetic transport and ordering phenomena in low dimensions, embedded in 3D extended oxides, are regarded as the microscopic origin for highly relevant macroscopic properties like superconductivity[1] or magneto resistance.[2] The best performing respective materials known display, as a common feature, randomly doped or substituted sublattices which breaks translational symmetry. This latter fact has considerably impaired stringent theoretical analyses and blurs experimental information by inhomogeneous signal broadening effects. For a better understanding of charge, spin and orbital ordering, as separate or coupled phenomena, it would be highly desirable to have intrinsically doped model systems at hand with well-defined chemical compositions and periodicities.

Recently, we have developed the azide/nitrate route as a convenient, versatile and prolific approach to the solid state synthesis of alkali oxometalates.[3] As one of the particular strengths of this technique, the oxygen content, and thus the valence state of, for example, a transition element included can be reliably and minutely adjusted by the azide/nitrate ratio applied for the starting mixtures. Using this procedure we have managed to provide two series of intrinsically doped transition metalates of general compositions A_xCuO_2 and A_xMnO_2, where A represents an alkali metal. The cuprates feature strands of edge sharing squares, which are centered by Cu^{2+} and Cu^{3+} in a fully charge ordered manner. They indeed can be regarded model systems for studying the order−disorder transitions mentioned above: $Na_3Cu_2O_4$[4] is a first unambiguous manifestation of a Wigner crystal,[5] while in $Na_5Cu_3O_6$ excitations across the Wigner gap affect antiferromagnetic ordering at low temperatures,[6] and $Na_8Cu_5O_{10}$[4] finally shows long-range collinear magnetic order with a spin density modulation caused by competing, weak interchain interactions.[7]

As a characteristic structural building principle, the more recent manganates(II/III) feature close packed channels with hexagonal cross sections, the corners of which are decorated with the alkali metals.[8] One-dimensional polyanionic chains $[MnO_2]^{n-}$ are running through the centers of the channels marked by the alkali ions. Since the periodicities of the alkali metal and manganate sublattices along the channels' direction are independent, the crystal structures can be regarded as composites. Indeed, some of them, like $Rb_{1.3711}MnO_2$,[8a] are appropriately described in higher dimensional space, others can be addressed by conventional crystallography in 3D, examples for the latter scenario are $Cs_4Mn_3O_6$[8b] or $Rb_{15}Mn_{11}O_{22}$.[8c] All new manganates show strong magnetic couplings, which might interestingly be mediated either by super exchange mechanisms or direct Mn−Mn interactions, and no discrete charge ordering is observed in any of them.

Here we report on a new candidate of the series, $Cs_3Mn_2O_4$, which shows for the first time in this class of materials complete charge ordering of Mn^{2+} and Mn^{3+}. It is strongly magnetically

Received: April 27, 2012
Published: June 25, 2012

   dx.doi.org/10.1021/ja303889g | J. Am. Chem. Soc. 2012, 134, 11734−11739

coupled already at ambient temperature and develops conspicuous field dependent magnetic ordering phenomena. Further, we analyze the experimental observations by density functional theoretical (DFT) calculations.

EXPERIMENTAL SECTION

Synthesis. $Cs_3Mn_2O_4$ was prepared via the azide/nitrate route[3] from Mn_2O_3 (99.9%, Chempur, Karlsruhe, Germany), $CsNO_3$ (99.9%, Acros Organics, Geel, Belgium) and CsN_3. This latter was prepared from aqueous HN_3 and $CsCO_3$ (99%, Sigma).[9] The starting materials were mixed in the molar ratio 11:1:3, according to the reaction

$$11CsN_3 + CsNO_3 + 3Mn_2O_3 \rightarrow 3Cs_3Mn_2O_4 + 3Cs + 17N_2$$

In a first step, the starting mixture was ground thoroughly in an agate mortar, pelletized under 10^5 N, dried in vacuum (10^{-3} mbar) at 400 K overnight and placed under argon in closed steel vessels provided with a silver inlay. These specially designed containers are equipped with squeeze seals, which withstand the internal pressure to a certain degree, but also let safely escape the considerable amounts of nitrogen formed during the reaction.[3] In a flow of dried argon, the following temperature program was applied: 298 K → 533 K (100 K/h); 533 K → 653 K (5 K/h); 653 K → 773 K (20 K/h) and subsequent annealing for 30 h at 773 K.

Hazards. The temperature control, as given above, must be strictly followed. Rapid heating or running the reaction in a gastight welded container can lead to a dangerous explosion!

The as-obtained product mixture, containing a black powder and elemental cesium, is very sensitive to humid air and therefore all further manipulations must be run in an inert atmosphere of purified argon. Single crystals of $Cs_3Mn_2O_4$ were grown by post annealing the as-obtained mixture in arc-welded tantalum ampules at 773 K for 500 h. Excess of cesium was removed from the final product by heating under vacuum at 373 K using a Schlenk tube fitted with a coldfinger.

X-Ray Diffraction. For X-ray diffraction, a single crystal was selected in a drybox (M. Braun, Garching, Germany) under an argon atmosphere (<0.1 ppm O_2, H_2O) and mounted in a sealed glass capillary. Collection of the diffraction intensities was performed at 298 K with a SMART-APEX-II CCD X-ray diffractometer (Bruker AXS, Karlsruhe, Germany) with graphite-monochromated Mo−Kα radiation (λ = 71.073 pm). The intensities were integrated with the SAINT subprogram of the Bruker Suite software package.[10] A multiscan absorption correction was applied using SADABS.[11] The structure was solved by direct methods and refined by full-matrix least-squares fitting with the SHELXTL software package.[12] It turned out, that the crystal under investigation, was pseudomerohedrally twinned, and the twin-law [0 0 1, 0 −1 0, 1 0 0] had to be applied during the final refinement, to obtain meaningful displacement parameters for the oxygen atoms. The R_1 values with and without twin-refinement are 0.0407 and 0.2480, respectively. Crystal data of $Cs_3Mn_2O_4$:[13] monoclinic, $P2_1/c$ (no. 14), a = 1276.33(1) pm, b = 1082.31(2) pm, c = 1280.29(2) pm, β = 118.390(2)° (lattice constants extracted from powder data), V = 1555.87(3) Å^3, ρ_{calc} = 4.89 g cm^3, Z = 8, ω-scan, 7872 symmetry independent reflections ($2\theta_{max}$ = 74.2°), 165 refined parameters. R_1 = 0.0407, wR_2 = 0.1199 (7439 $F_0 > 4s(F_0)$); R_1 = 0.0426, wR_2 = 0.1209 (all data). Further details on the crystal structure analysis can be obtained from Fachinformationszentrum Karlsruhe, 76344 Eggenstein-Leopoldshafen, Germany (http://www.fiz-karlsruhe.de/request for deposited data.html) on quoting the CSD number: CSD-424542. Further details may be also obtained from Supporting Information.

X-ray powder diffractograms of the final product were recorded at room temperature on a laboratory powder diffractometer (D-8, Bruker, with Mo−Kα_1 radiation, λ = 70.9300 pm) in Debye−Scherrer geometry. For this purpose the sample was sealed in a borosilicate glass capillary and the data were collected in the 2θ range from 3° to 40°. The XRPD pattern was analyzed by the Le Bail profile analysis using the software package TOPAS.[14]

Magnetic Measurements. Magnetic properties were studied in a Quantum Design MPMS7 SQUID Magnetometer. Zero-field-cooled (ZFC) and field-cooled (FC) magnetic susceptibility data were obtained under different fields 10^{-3} T ≤ H ≤ 7 T in the temperature range 2 K ≤ T ≤ 600 K. Hysteresis loops in ZFC conditions were obtained at temperatures 2.5 K ≤ T ≤ 300 K varying the field up to ±7 T.

Theoretical Methods. First principles density functional theory (DFT) calculations at 0 K were carried out to investigate the electronic and magnetic structure of $Cs_3Mn_2O_4$. The structural parameters are taken from the experimental X-ray single crystal data. The calculations were performed using Vienna *ab initio* simulation package (VASP),[15] employing the Perdew-Burke-Ernzerhof (PBE) exchange-correlation functional of generalized gradient approximation (GGA).[16] The core−valence electron interaction was treated by all-electron projector-augmented wave method (PAW).[17] The PAW potentials present the valence electrons of Cs ($5s^2$, $5p^6$, $6s^1$), Mn ($3d^6$, $4s^1$), and O ($2s^2$, $2p^4$). The cutoff energy for the expansion of the wave function into plane waves was set to 400 eV. The Brillouin-zone integration was sampled using a 4 × 4 × 4 k-point mesh generated by Monkhorst-Pack scheme. The electronic occupancies were determined by the Gaussian smearing method with the width of smearing set to 0.05 eV. The electronic and spin degrees of freedom are left free to change until the self-consistence convergence of 0.1 × 10^{-6} eV was achieved. In the convergence process particular attention was paid to the initial spin moment in different magnetic ordered structures. The initial magnetic configurations were legitimately constituted by the judicious choice of the Mn magnetic configuration based on the formal oxidation states assigned to Mn in $Cs_3Mn_2O_4$ based on the local coordination geometries. The total and spin moment per atom was calculated by integrating the spin density within the Bader atomic basins.[18]

RESULTS AND DISCUSSION

Synthesis. $Cs_3Mn_2O_4$ has been synthesized fully reproducibly along the azide/nitrate route, with a slight change compared to the standard procedure.[3] Instead of precisely weighing out the starting materials, here an excess of CsN_3 was applied, which has improved phase purity and crystallinity of the final product. Excessive elemental cesium was quantitatively distilled off in vacuum.

The black title compound is sensitive to humid air. The powder X-ray diffraction pattern is shown in Figure 1. It can be indexed in a monoclinic crystal system, lattice parameters obtained are given above.

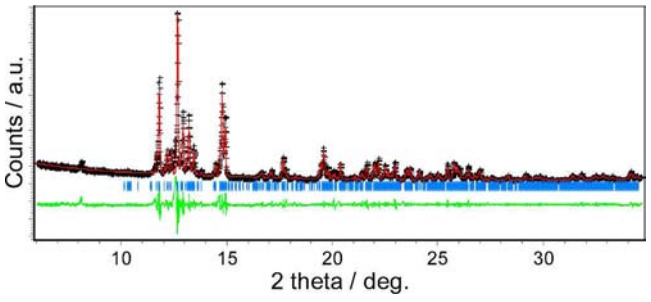

Figure 1. Room temperature XRPD pattern of $Cs_3Mn_2O_4$ and corresponding LeBail fit. Key: observed data (+) and calculated profile (solid line); the difference plot is drawn below the profile. Tick marks indicate peak positions of the $Cs_3Mn_2O_4$ compound.

Crystal Structure. The room temperature structure of $Cs_3Mn_2O_4$ was elucidated from single-crystal X-ray diffraction data collected at 298 K. The structural parameters, atomic coordinates, representative interatomic distances, and isotropic displacement parameters, are given in Supporting Information. As shown in Figure 2, the crystal structure is characterized by the presence of virtually one-dimensional polyanions $MnO_2^{1.5-}$ constituted of edge-sharing, distorted MnO_4 tetrahedra. Such

dx.doi.org/10.1021/ja303889g | J. Am. Chem. Soc. 2012, 134, 11734−11739

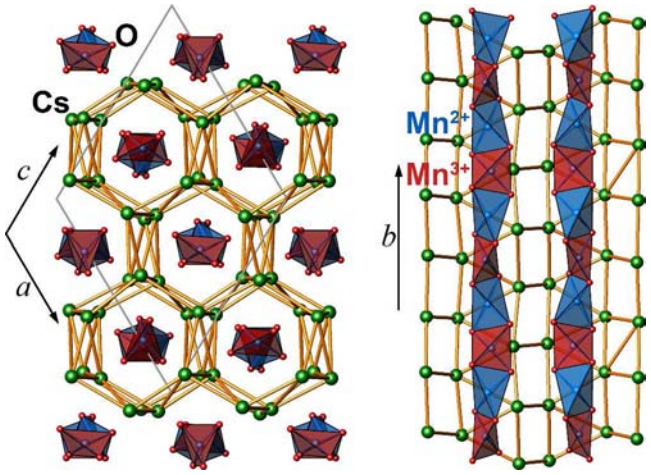

Figure 2. (Left) Projection of the crystal structure of $Cs_3Mn_2O_4$, view along [0 1 0] direction, with margins of the unit cell (gray). (Right) Fragment of the crystal structure. Color code: MnO_4 tetrahedra (blue Mn^{2+}, red Mn^{3+}), shortest distances between cesium atoms (green) are emphasized by orange sticks.

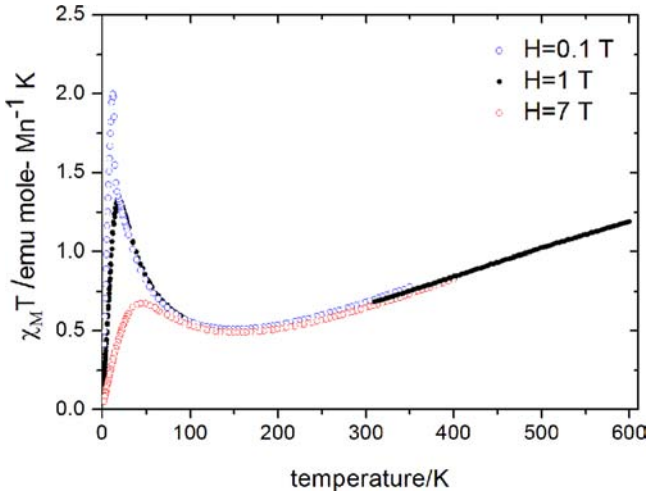

Figure 3. Plot of $\chi_M T$ versus temperature.

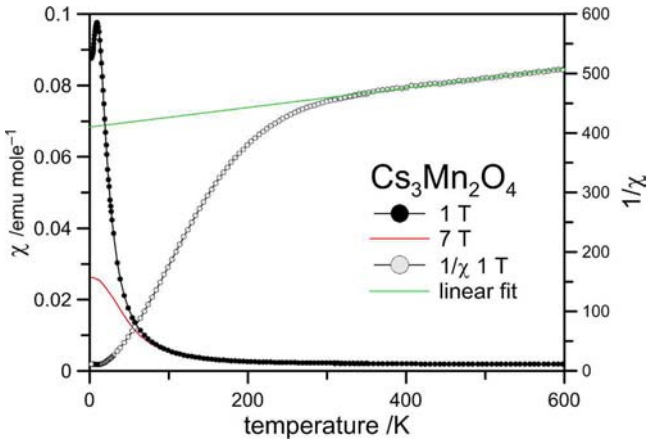

Figure 4. Susceptibility and inverse susceptibility versus temperature.

chains run parallel to the *b* axis of the monoclinic structure, and are separated by cesium ions, which form a distorted honeycomb-like arrangement of channels. These basic structural principles correspond to those previously found for $K_{29}Mn_{17}O_{34}$, $Rb_{11}Mn_8O_{16}$, and $Cs_4Mn_3O_6$.[8]

The new oxide thus shows a pronounced one-dimensional character: the intrachain Mn−Mn distances alternate between 276 and 279 pm, values which are rather short and exceed the Mn−Mn distance found in metallic manganese by less than 10%. In contrast, the interchain Mn−Mn distances are substantially larger (minimal separation: 600 pm). As for the coordination environments of the manganese ions, one can distinguish two types of distorted MnO_4 tetrahedra, displaying two sets of Mn−O distances ranging from 189 to 192 pm (Mn1, Mn2) and 202−208 pm (Mn3, Mn4), respectively. Such a structural condition is indicative for charge ordering, and the oxidation states 3+ and 2+ can be unambiguously assigned to each manganese atom position by analyzing the Mn−O bond distances. In contrast to previously reported $Cs_4Mn_3O_6$, $Rb_{11}Mn_8O_{16}$, and $Rb_{15}Mn_{11}O_{22}$ compounds,[8] where the ordering of Mn^{2+}/Mn^{3+} can be described best in the sense of a charge density wave,[8a] a real charge ordering is observed in $Cs_3Mn_2O_4$ with Mn^{2+} and Mn^{3+} alternating along the MnO_2 chains (−Mn^{3+}− Mn^{2+}− Mn^{3+}− Mn^{2+}−, Figure 2, right), which is similar to the Cu^{2+}/Cu^{3+} ordering scheme as observed in $Na_3Cu_2O_4$.[4] The MnO_2 chains are adjusted in a way, that Mn^{3+} and Mn^{2+} positions in adjacent chains are located at the same level in *b*-direction (Figure 2, right).

Magnetic Measurements. The main results of the magnetic studies carried out in this compound are shown in Figures 3−5. As can be seen in Figure 3, at high temperature the value of the $\chi_m T$ product (1.22 emu mol Mn^{1-} K at T = 600 K and 0.77 emu mol Mn^{1-} K at 300 K) is considerably lower than expected for a 50:50% ratio of uncoupled high spin Mn^{2+} and Mn^{3+} ions (3.13−3.67 emu mol Mn^{1-} K).[19] Such small values together with the continuous diminution of $\chi_m T$ as temperature decreases reveal dominating antiferromagnetic exchange couplings between the manganese ions, which is confirmed by the plot of the reciprocal of the molar magnetic susceptibility versus temperature. As shown in Figure 4, linear fitting of the data above 350 K affords very good agreement to a Curie−Weiss behavior [$\chi = C/(T-\theta)$] from which a very high negative value of θ = −2500 K and an increased C = 5.73 emu mol Mn^{1-} K are calculated.

However, the upward trend of the $\chi_m T$ product below ∼150 K, that is initially smooth but rather pronounced below ∼60 K and gives rise to a peak which is more distinct for lower field strengths ($\chi_m T_{max}$ being 2 emu mol^{-1} K at T = 12 K under H = 0.1 T), suggests the existence of a ferromagnetic component.[20] According to the above observation and the field dependence of the magnetization below 12 K, see below, the magnetic behavior should be either ferrimagnetic or canted antiferromagnetic.[21] As for the second drop of $\chi_m T$ observed at lower temperatures, it may arise from increasing antiferromagnetic interactions and/or saturation effects.[22] In this context, it should be mentioned that the magnetization at low temperature is seen to be both, field and history dependent. For example when measured under high magnetic fields, both the FC and ZFC $\chi_m T$ curves slightly diverge while showing a peak at T ∼12 K (Figure S1, Supporting Information), that reminds of the typical signature for an antiferromagnetic transition at the Néel temperature. Nevertheless, the ZFC and FC χ_m(T) curves measured under low fields show an abrupt increase below ca. 13 K, followed by a marked divergence below 12 K as the ZFC curve peaks at this temperature while the FC one keeps increasing upon further cooling (Figure S2, Supporting

dx.doi.org/10.1021/ja303889g | J. Am. Chem. Soc. 2012, 134, 11734−11739

Information). This irreversible behavior may arise from the onset of long-range 3D ordering due to interchain interactions. Also, the observed magnetization field dependence suggests weak ferromagnetism or canted antiferromagnetism in the compound.[22]

To deepen further in the nature of the low temperature phase, we have measured its isothermal magnetization as a function of field at different temperatures (Figure 5). As it can

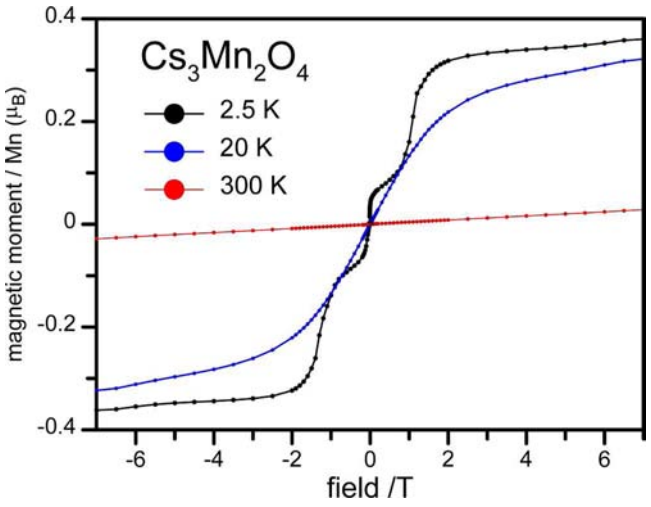

Figure 5. Isothermal magnetization as a function of field at different temperatures.

be seen, for $T < T_N$ the magnetization measurements display unusual hysteresis curves and reveal the presence of a metamagnetic transition in two steps: starting from zero field, the first step occurs inmediately with increasing field followed by a second step at higher fields. No further transitions are observable up to 7 T.

The magnetization of the intermediate phase reaches a value that is about 1/3 of that observed at the highest measured field (7 T), $M_{max} = 0.36\ \mu_B$, a value that is far below the saturation value expected for a 50:50 Mn^{2+}/Mn^{3+} system (4.5 μ_B). This result confirms the presence of strong antiferromagnetic interactions in the sample, which the field is incapable of completely overcoming.

The initial abrupt increase of the magnetization at low field and its almost linear variation for $H > 2$ T again reminds of that shown by weak ferromagnets or canted antiferromagnets, even if the second step indicates the presence of an additional field induced magnetic transition and a more complex situation. In connection with the former, a small hysteresis is seen below 2 T, which supports the presence of a certain ferromagnetic component (see Supporting Information, Figure S3). The remnant magnetization is $3.61 \times 10^{-2}\ \mu_B$ and the observed value for the coercive field is about 0.02 T. Taking into account that for weak ferromagnetism arising from spin canting, the canting angle α is related to M_R and M_S through $\sin(\alpha) = M_R/M_S$,[23] an α of ~0.05° can be estimated. On the other hand, and as can be seen in Figure 5, the isothermal magnetization measured at $T = 20$ K shows a S-shape dependence on the magnetic field, that is consistent with the coexistence of ferromagnetic and antiferromagnetic interactions. Meanwhile, for $T > 100$ K the values of the magnetization continue to decrease and they show an almost linear dependence with the field.

With all this information in hand, and taking into account the structural features of this compound, we explain the observed magnetic behavior as follows: the dominant magnetic exchange interactions, that are antiferromagnetic, occur between the Mn ions within a chain (intrachain interactions), while the magnetic interactions between the chains (interchain interactions) are expected to be comparatively weaker. Within a chain, the Mn−Mn distances are slightly longer, even if close, to the critical distance to allow for significant direct Mn−Mn magnetic exchange[24] thus suggesting that the main coupling will occur via intervening oxygen anions. As each [MnO_4] tetrahedron shares a common edge with two neighbors, the Mn−O−Mn superexchange—with cation−anion−cation angles in the range of 87.7−90.3°—results in antiferromagnetic interactions, as predicted by the Goodenough-Kanamori coupling rules.[25] Nevertheless, due to the different magnetic moments on the Mn^{2+} and Mn^{3+} ions the chains turn to be ferrimagnetic. In addition, as these are not strictly linear but slightly undulating, the AF alignment of the magnetic moments along the chains is not completely antiparallel, which results in a small canting.

Finally 3D magnetic ordering between the chains seems to take place at lower temperature (T ~12 K), and the different 3D magnetic structures that can appear, depending on the field, are probably the result of different AF or ferromagnetic alignments among the MnO_2 chains.

Band Structure Calculations. In order to shed further light on the electronic structure and magnetic ordering of $Cs_3Mn_2O_4$, we performed DFT calculations. Table 1 lists the

Table 1. Calculated Magnetic Moments, Band Gaps and Total Energies for $Cs_3Mn_2O_4$ Crystal Structure in Different Magnetic Order States[a]

	Mn^{2+}	Mn^{3+}	μ_B/Mn	E_g /eV	E /eV
NSP	1.02	1.17	0.00	0.00	26.47
FM	4.38	3.54	3.96	0.40	3.99
AFM1	4.20	3.31	0.44	0.40	2.53×10^{-3}
AFM2	4.20	3.31	0.00	0.51	0.00
AFM3	4.38	3.54	0.00	0.40	3.95

[a]AFM1, AFM in the chains and FM between the chains (ferri); AFM2, AFM in and between the chains; AFM3, FM in the chains and AFM between the chains; NSP, Non spin polarized situation.

calculated results on the experimental monoclinic crystal structure, suggesting that at 0 K $Cs_3Mn_2O_4$ stabilizes in an antiferromagnetic state—AFM2 (ferri- and antiferromagnetic coupling in and between the chains, respectively). However, if spin ordering is ferromagnetically coupled between the chains, $Cs_3Mn_2O_4$ adopts a ferrimagnetic state (AFM1). This is 2.53 meV/unit cell above the AFM2 ordering. Fundamentally, the two magnetic structures are energetically degenerate which is in perfect agreement with the experimental findings. According to experimental magnetic measurements, the field required for the AFM2 to AFM1 transition is about 2.5 T (at 2.5 K). The spin moments per Mn site (Mn^{2+}: 4.20, Mn^{3+}: 3.31, and μ_B/Mn: 0.44) supports the experimental moment 0.36 μ_B/Mn. The ferromagnetic (FM) order in and between the MnO_2 chains is far above (3.99 eV) the AFM state.

We also constructed another magnetic order state that contains FM and AFM order in and between the chains respectively. This order state (AFM3) is energetically closer to the FM state, but 43 meV lower in energy. This indicates the interchain coupling is rather weak. However, at low temper-

dx.doi.org/10.1021/ja303889g | J. Am. Chem. Soc. 2012, 134, 11734−11739

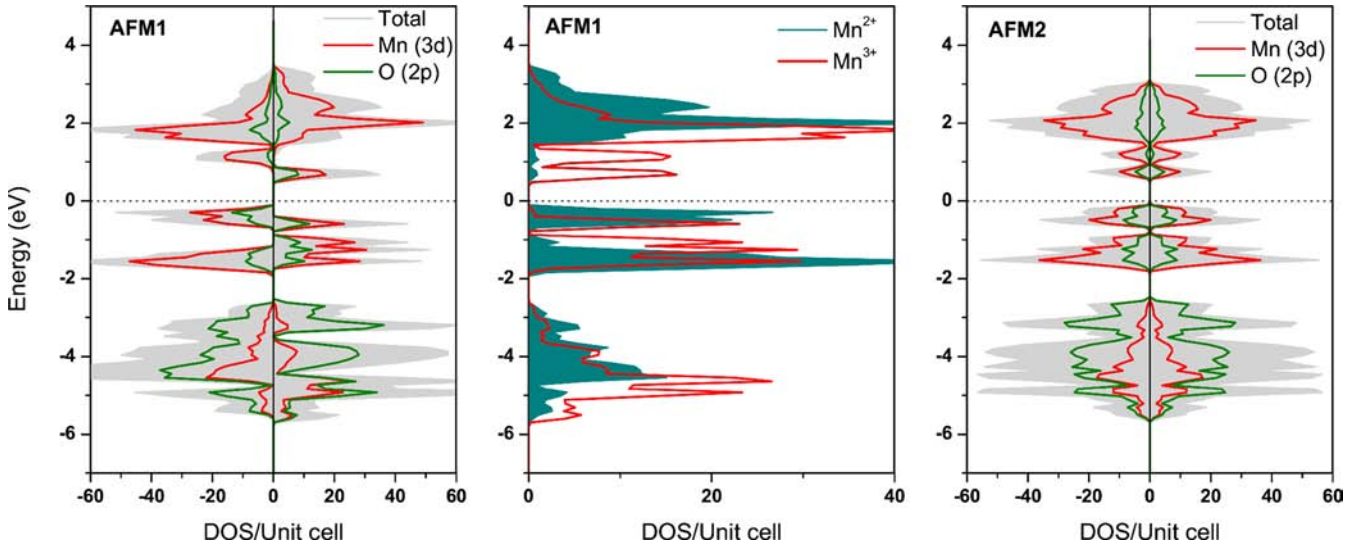

Figure 6. Electronic total and projected DOS for $Cs_3Mn_2O_4$ in AFM1 (left) and AFM2 (right) states. Mn site projected DOS for AFM1 state is depicted in the middle diagram.

ature the small amount of exchange energy substantially influences the spin ground state structure as we have seen in our present experiments.

A finite DOS is present at the Fermi level (E_F) for a nonspin polarized situation implying a metallic character, see Figure S4 (Supporting Information). In all spin polarized magnetic order structures, a small insulating band gap of about 0.4 eV is opened. Here, we will describe the electronic structure of AFM1 and AFM2 in detail as these are the ground state magnetic order structures for $Cs_3Mn_2O_4$. See Supporting Information for other magnetic and nonmagnetic cases.

As a whole, the DOS is similar in both AFM1 and AFM2 as shown in Figure 6. The partial DOS(PDOS) analysis shows that Mn *d* states are mainly presented near the E_F with overlap of O states in both the spin up/down channels. In AFM1 the asymmetric PDOS indicates ferrimagnetic character with an increased band gap by order of 2 from each similar spin-channels. There is a very small energy gap between e_g and t_{2g} states which supports the high-spin state of Mn in $Cs_3Mn_2O_4$. The Mn site projected DOS based on formal oxidation states vindicates the ferrimagnetic order. This picture also makes clear that the ferrimagnetic ordering is lifted by the Mn^{2+} sites.

CONCLUSION

The new one-dimensional Manganite $Cs_3Mn_2O_4$ was synthesized via the azide/nitrate route, and its crystal structure solved from room temperature single-crystal X-ray diffraction data. The structural data and calculated magnetic moments per Mn site of $Cs_3Mn_2O_4$ clearly confirm complete charge ordering, and the oxidation states of 2+ and 3+ can be assigned to the different Mn positions, alternating along the chain direction. The computed energies and band structures of different spin ordered states, together with the experimental observation of coupled magnetic behavior, give a consistent picture of the magnetic structure: up to high temperatures antiparallel orientation of the spins along the chain direction due to strong intrachain AF coupling between Mn^{2+} and Mn^{3+}. Below the Néel temperature (T_N) ~12 K, long-range 3D ordering of such ferrimagnetic chains, in accordance with the energetically more favorable antiferromagnetic interchain couplings, is changing into ferromagnetic upon application of a strong enough magnetic field.

ASSOCIATED CONTENT

Supporting Information

Detailed Crystallographic data, further susceptibility curves and DOS diagrams. This material is available free of charge via the Internet at http://pubs.acs.org.

AUTHOR INFORMATION

Corresponding Author

*M.Jansen@fkf.mpg.de.

Notes

The authors declare no competing financial interest.

ACKNOWLEDGMENTS

M.A.S.R. is grateful to Ministerio de Economía y Competitividad MINECO (Spain) under project FEDER MAT2010-21342-C02-01.

REFERENCES

(1) Cava, R. E. *J. Am. Ceram. Soc.* **2000**, *83*, 5−28.
(2) Rao, C. N. R.; Mahesh, R.; Raychaudhuri, A. K.; Mahendiran, R. *J. Phys. Chem. Solids* **1998**, *59*, 487−501.
(3) (a) Trinschek, D.; Jansen, M. *Angew. Chem.* **1999**, *111*, 234−235; *Angew. Chem., Int. Ed.* **1999**, *38*, 133−135. (b) Jansen, M. *Z. Anorg. Allg. Chem.* **2012**, *638*, No. 10.1002/zaac.201200275.
(4) Sofin, M.; Peters, E. M.; Jansen, M. *J. Solid State Chem.* **2005**, *178*, 3708−3714.
(5) Horsch, P.; Sofin, M.; Mayr, M.; Jansen, M. *Phys. Rev. Lett.* **2005**, *94*, 076402.
(6) Ali, N. Z.; Sirker, J.; Nuss, J.; Horsch, P.; Jansen, M. *Phys. Rev. B* **2011**, *84*, 035113.
(7) Raichle, M.; Reehuis, M.; André, G.; Capogna, L.; Sofin, M.; Jansen, M.; Keimer, B. *Phys. Rev. Lett.* **2008**, *101*, 0472002.
(8) (a) Nuss, J.; Pfeiffer, S.; van Smaalen, S.; Jansen, M. *Acta Crystallogr. Sect. B* **2010**, *66*, 27−33. (b) Pfeiffer, S.; Nuss, J.; Jansen, M. *Z. Anorg. Allg. Chem.* **2010**, *636*, 23−29. (c) Pfeiffer, S.; Nuss, J.; Jansen, M. *Z. Kristallogr. New Cryst. Struct* **2009**, *224*, 377−378.
(9) Brauer, G. *Handbuch der Präparativen Anorganischen Chemie*, 3rd. ed.; Enke: Stuttgart, 1975; Vol. *1*, p 458.

(10) Bruker Suite, version 2008/3; Bruker AXS Inc.: Madison, WI, 2008.
(11) Sheldrick, G. M. *SADABS — Bruker AXS Area Detector Scaling and Absorption*, version 2008/1; University of Göttingen, Germany, 2008.
(12) Sheldrick, G. M. *Acta Crystallogr., Sect. A* **2008**, *64*, 112−122.
(13) Further details of the crystal structure investigations may be obtained from the Fachinformationszentrum Karlsruhe, 76344 Eggenstein-Leopoldshafen, Germany (fax (+49)7247-808-666; e-mail crysdata(at)fiz-karlsruhe.de) on quoting the depository number CSD-424542.
(14) *Topas*, version 4.1; Bruker AXS: Karlsruhe, Germany, 2007.
(15) Kresse, G.; Furthmüler, J. *Phys. Rev. B* **1996**, *54*, 11169.
(16) Perdew, J. P.; Burke, K.; Ernzerhof, M. *Phys. Rev. Lett.* **1996**, *77*, 3865.
(17) (a) Blöchl, P. E. *Phys. Rev. B* **1994**, *50*, 17953. (b) Kresse, G.; Joubert, D. *Phys. Rev. B* **1999**, *59*, 1758.
(18) Tang, W.; Sanville, E.; Henkelman, G. *J. Phys.: Condens. Matter* **2009**, *21*, 084204.
(19) Carlin, R. L. *Magnetochemistry*; Springer: Berlin, 1986.
(20) Sanz, F.; Parada, C.; Rojo, J. M.; Ruíz-Valero, C. *Chem. Mater.* **2001**, *13*, 1334−1340.
(21) Yang, M.; Yu, J.; Shi, L.; Chen, P.; Li, G.; Chen, Y.; Xu, R. *Chem. Mater.* **2006**, *18*, 476−481.
(22) Han, S.; Manson, J.; Kim, J.; Miller, J. S. *Inorg. Chem.* **2000**, *39*, 4182−4185.
(23) Hahn, O. *Magnetism*; VCH: New York, 1993.
(24) Goodenough, J. B. *Prog. Solid State Chem.* **1971**, *5*, 145−399.
(25) (a) Goodenough, J. B. *Magnetism and the Chemical Bond*; Interscience: New York, 1963. (b) Kanamori, J. *J. Phys. Chem. Solids* **1959**, *10*, 87−98.